

# Analysis of plasmon resonance and surface-enhanced Raman scattering on periodic silver structures

M. Kahl and E. Voges

*Lehrstuhl für Hochfrequenztechnik, Universität Dortmund, 44221 Dortmund, Germany*

(Received 11 November 1999; revised manuscript received 1 February 2000)

Surface plasmon excitation and surface-enhanced Raman scattering (SERS) are investigated for periodic grating-type substrates such as binary silver gratings and silver gratings on silica. Electromagnetic near fields are calculated by an efficient implementation of a Rayleigh-expansion technique for rectangular-groove gratings. Far-field signals of Raman-active molecules adsorbed at the grating surface are determined by application of the Lorentz reciprocity theorem. SERS enhancement factors are considered for different types of gratings and for structures with different dimensions with respect to both the intensity and angular width of the emitted Stokes light. Thus, consideration of plasmon resonance widths leads to optimum structures for periodic SERS substrates if realistic experimental configurations involving a lens for detection are taken into account. For binary silver gratings, optimum grating depths of more than 80 nm are proposed for SERS measurements in a realistic experimental configuration, whereas maximum SERS signals are emitted into a single direction at shallow gratings with depths between 10 nm and 20 nm. Furthermore, silica gratings with isolated silver layers are superior to binary silver gratings. Due to both the large intensity and angular width of the emitted signals, SERS enhancement factors are additionally increased on such structures.

## I. INTRODUCTION

Grating-type substrates with nanometer dimensions offer the possibility of enhancing the electromagnetic field close to surfaces by factors up to  $10^3$  due to surface plasmon excitation.<sup>1</sup> Thereby, Raman signals from molecules adsorbed at these substrates are enhanced by up to six orders of magnitude. This surface-enhanced Raman scattering<sup>2,3</sup> (SERS) offers high sensitivity and the possibility of detecting monolayers of molecules. For this reason and the additional typical high selectivity of Raman scattering due to the fingerprint nature of the detected spectra, SERS has a large potential for new developments in chemical sensor applications.<sup>4-6</sup>

However, the excitation of surface plasmons by light requires special experimental configurations for flat metal surfaces like attenuated total reflection couplers<sup>1</sup> or rough surface structures. Suitable SERS substrates are, for example, electrochemically roughened silver electrodes, metal island films, metal colloidal films, and other roughened surfaces.<sup>7</sup> In contrast to these irregular substrates, regularly arranged particles and metallic gratings offer the possibility for a more systematic and reproducible study of the plasmon resonance contribution to SERS. Silver gratings or silver nanoparticles on crossed gratings of silica posts have been prepared by holographic<sup>8-12</sup> or *e*-beam lithography,<sup>13,14</sup> consecutive pattern transfer by etching, and final evaporation of a silver layer. Furthermore, suitable SERS substrates have been produced by replicating the silica posts into polyvinyl chloride (PVC) and evaporating silver on the PVC posts.<sup>15</sup> Electron-beam lithography has also been used to produce regular arrays of nanoparticles on flat surfaces by lift-off techniques.<sup>13,14</sup> These periodic SERS substrates can be fabricated with reproducibly and independently varied structural parameters such as grating period or height of the particles.

In this way, substrates with the structural dimensions required for optimum SERS enhancement can be fabricated. As the optimum surface structure depends on the kind of application, e.g., detection of SERS signals in forward or backward scattering geometry, suitable numerical methods are required to calculate the optimum surface topology in each case.

The well-defined topology of silver gratings<sup>12,16</sup> and nanoparticle arrays<sup>9,17</sup> has already been used for quantitative comparison of theory and experiment. Numerical calculations in this investigation as well as in different studies concerning the optimum grating height<sup>18</sup> are based on the expansion of the electromagnetic fields into Bloch waves. This method is known as the Rayleigh-expansion method.<sup>19</sup> SERS enhancement factors on regularly arranged nanoparticles have been calculated by a different approach applying an extended single-particle model.<sup>17</sup> Electromagnetic enhancement factors of about  $10^4$  have been calculated for both gratings and nanoparticle arrays.

In this paper we investigate one-dimensional (1D) rectangular-groove binary silver gratings, silver gratings on flat silica substrates, and silver layers on silica gratings (see Fig. 1). Silver is used because it is the most efficient SERS metal due to its dielectric properties.<sup>2</sup> The calculations are restricted to TM-polarized light because surface plasmon excitations require this polarization.<sup>1</sup> Therefore, a Rayleigh-expansion technique that is optimized for this polarization and rectangular metal gratings is used. Raman scattering is treated classically by assuming dipoles oscillating at the Stokes frequency with a dipole moment proportional to the local electric field. The far-field Raman signal of the radiating dipoles is calculated by a combination of Rayleigh expansion and the Lorentz reciprocity theorem. An efficient implementation of this method allows one to calculate the enhancement for different types and geometries of gratings. We discuss in detail the influence of angle of incidence  $\theta_0$

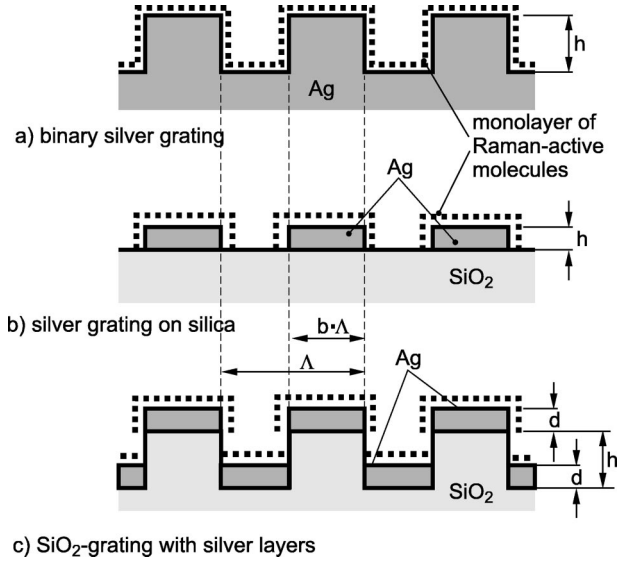


FIG. 1. Different types of rectangular-groove grating structures investigated: (a) binary silver grating, (b) silver grating on a silica substrate, and (c) silica grating with silver layers on top of the ridges and on the bottom of the grooves. The dotted lines indicate the adsorption sites of the Raman-active molecules.

and detection angle  $\theta_s$ , grating period  $\Lambda$ , ratio of grating ridge width to grating period  $b$ , and grating depth  $h$  on both plasmon resonance and SERS enhancement for various types of gratings. SERS enhancement factors are defined by comparing far-field Raman signals from oscillating dipoles on gratings and in liquids. The results are compared to other theoretical investigations and to experimental results.

## II. THEORY

### A. Calculation of electric near fields

There exist various methods to calculate the expansion coefficients of the Rayleigh method.<sup>19</sup> In order to study the diffraction of TM-polarized plane waves on rectangular-groove gratings the expansion coefficients are calculated by a rigorous coupled wave analysis (RCWA).<sup>20</sup> Due to the convergence problem of this formalism for TM polarization<sup>21</sup> an improved method is used.<sup>22,23</sup> For completeness a short outline of Rayleigh expansion and the improved RCWA is given.

A TM-polarized plane wave with a magnetic field

$$H_{inc,z} = \exp[-jk_0 n_1 (\sin \theta_0 x - \cos \theta_0 y)] \quad (1)$$

is incident with an angle  $\theta_0$  on a rectangular metallic grating with grating period  $\Lambda$  and groove depth  $h$  (Fig. 2).

In regions I and II the diffracted field can be expanded into plane waves:<sup>19</sup>

$$H_{I,z} = H_{inc,z} + \sum_{m=-N}^N R_m \exp[-j(k_{xm}x + k_{I,ym}y)], \quad (2)$$

$$H_{II,z} = \sum_{m=-N}^N T_m \exp[-j(k_{xm}x - k_{II,ym}y)], \quad (3)$$

where  $R_m$  and  $T_m$  are the Rayleigh coefficients corresponding to the reflected and transmitted diffraction order  $m$ . The  $x$

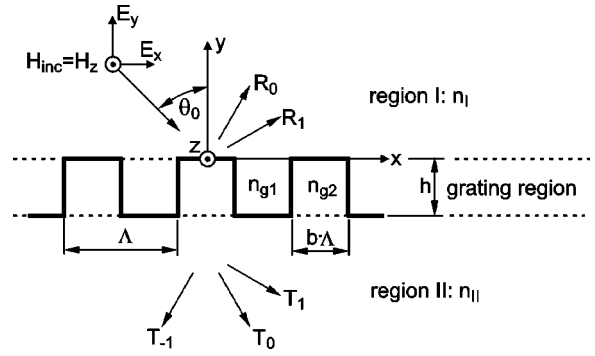


FIG. 2. Grating geometry of the diffraction problem used for calculation by Rayleigh-expansion technique. The incident TM-polarized field is diffracted into plane waves with coefficients  $R_m$  (reflected field) and  $T_m$  (transmitted field) in regions I and II. The material properties of the different regions are given by their corresponding refraction indices  $n$ .

component  $k_{xm}$  of the wave vector is determined in both regions by the Floquet condition,

$$k_{xm} = k_0 \left( n_1 \sin \theta_0 - m \frac{\lambda}{\Lambda} \right). \quad (4)$$

The  $y$  component  $k_{ym}$  follows from the separation condition,

$$k_{\zeta,ym} = \sqrt{(k_0 n_\zeta)^2 - k_{xm}^2}, \quad (5)$$

where  $\zeta = I$  or  $\zeta = II$  denotes the corresponding region. For complex  $k_{ym}$  the root that results in evanescent waves has to be taken. A plane wave expansion with constant coefficients is not valid in the grating region. There, the expansion

$$H_{gz} = \sum_{m=-N}^N U_m(y) \exp(-jk_{xm}x) \quad (6)$$

is used. The coefficients  $U_m(y)$  are calculated by solving Maxwell equations in the quasi-plane-wave basis. Within the grating region the periodic relative permittivity  $\epsilon = n^2$  is a function of  $x$  only, because rectangular-groove gratings are considered. Therefore,  $\epsilon$  and its reciprocal  $1/\epsilon$  are expanded in Fourier series with constant Fourier coefficients. Then the Maxwell equations in the quasi-plane-wave basis result in a set of second-order differential equations with constant coefficients,

$$k_0^{-2} \frac{\partial^2 \vec{U}}{\partial y^2} = \hat{M} \vec{U}, \quad (7)$$

which can be solved analytically. The definition of the matrix  $\hat{M}$  and a detailed step-by-step guide for the numerical implementation are given in Refs. 20 and 22. The boundary conditions for the differential equations are determined by the continuity equations for  $H_z$  and  $E_x$  at  $y=0$  and  $y=-h$ . Thus, the coefficients  $R_m$ ,  $T_m$ , and  $U_m(y)$  and thereby the magnetic field can be computed in each region. The corresponding electric field components are calculated from the Maxwell equations by evaluating the analytical derivatives of the expansion of  $H_z$  in the different grating regions. This yields expansions for  $E_x$  and  $E_y$  similar to Eqs. (2), (3), and (6) with additional factors due to the derivatives of the ex-

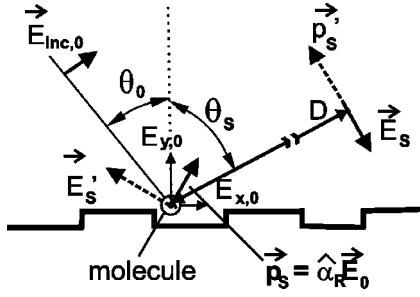


FIG. 3. Application of Lorentz reciprocity theorem.

ponential function. However, the number of expansion coefficients has to be increased because the convergence for electric fields in the grating region is slower than for  $H_{gz}$ .

The algorithm described can be used for the numerical simulation of binary silver gratings [Fig. 1(a)] and of silver gratings on silica substrates [Fig. 1(b)]. The  $\text{SiO}_2$  gratings involve a more complicated grating region, which is built up of three single grating layers [Fig. 1(c)]. Nevertheless, the algorithm can be simply extended for this problem. The differential Eq. (7) is deduced three times with three different Fourier series for  $\epsilon(x)$  and  $1/\epsilon(x)$  in the different grating layers. Solutions of the differential equations are calculated for each grating layer and are used to expand the magnetic and electric fields. Then three sets of coefficients  $U_m(y)$  as well as the Rayleigh coefficients are determined by the boundary conditions at  $y=0$ ,  $y=d$ ,  $y=h$ , and  $y=d+h$ . The corresponding linear equation system is solved numerically. The computational times of these numerical calculations depend on the third power of the matrix dimension, which is three times larger for the  $\text{SiO}_2$  gratings. Therefore, the number of retained Rayleigh coefficients has to be reduced in comparison to silver gratings for comparable computing times.

### B. Surface-enhanced Raman scattering

The above algorithm allows the calculation of the electric field at the adsorption sites of the molecules. Raman scattering is considered classically.<sup>24</sup> The electric near field  $\vec{E}_0$  at frequency  $\omega_0$  induces an oscillating dipole

$$\vec{p}_s = \hat{\alpha}_R \vec{E}_0 \quad (8)$$

radiating at the shifted Stokes frequency  $\omega_s = \omega_0 - \omega_{\text{mol}}$ . As one-dimensional gratings are considered, the Raman polarizability tensor  $\hat{\alpha}_R$  has only  $2 \times 2$  components.

The oscillating dipole is located close to the silver surface. Therefore, the radiated dipole fields again couple to surface plasmons. One solution for this problem is the application of the Lorentz reciprocity theorem.<sup>16,25</sup> A virtual dipole  $\vec{p}_s'$  is considered at the location of the detector in the far field (see Fig. 3).

The distance  $D$  between the detector and the grating surface is much larger than the Stokes wavelength  $\lambda_s$  of the virtual dipole. Therefore, the light emitted by the virtual dipole is incident as a plane wave on the grating and the algorithm of Sec. II A can be used to obtain the field  $\vec{E}_s'$  of the virtual dipole  $\vec{p}_s'$  at the location of the real dipole  $\vec{p}_s$ . Con-

sequently, the required far field  $\vec{E}_s$  of  $\vec{p}_s$  can be calculated from the Lorentz reciprocity theorem

$$\vec{p}_s' \cdot \vec{E}_s = \vec{E}_s' \cdot \vec{p}_s. \quad (9)$$

When aligning  $\vec{p}_s'$  parallel to  $\vec{E}_s$  the left-hand product can be written as  $|\vec{p}_s'| \cdot |\vec{E}_s|$  and Eq. (9) is divided by  $|\vec{p}_s'|$ . The power density of the incident plane wave from the virtual dipole at a distance  $D$  at an angle perpendicular to the dipole axis is given by<sup>26</sup>

$$S_{\text{dipole}} = \frac{\pi^2 c}{2 \epsilon_0 \lambda^4 D^2} p^2. \quad (10)$$

Thus, the dipole moment  $|\vec{p}_s'|$  is calculated from

$$|\vec{p}_s'| = \frac{\epsilon_0 \lambda_s^2 D E_0}{\pi} \quad (11)$$

in dependence on the incident field  $E_0$  that has been used for the near-field calculation by the rigorous coupled wave analysis. Therefore, the power density  $S_{\text{SERS,mol}} = \frac{1}{2} \sqrt{\epsilon_0 / \mu_0} |E_s|^2$  of the SERS signal of a single molecule is

$$S_{\text{SERS,mol}} = \frac{1}{2} \sqrt{\frac{\epsilon_0}{\mu_0}} \frac{\pi^2 |\vec{E}_s' \cdot \hat{\alpha}_R \cdot \vec{E}_0|^2}{\epsilon_0^2 \lambda_s^4 D^2 E_0^2}. \quad (12)$$

In order to consider enhancement factors for the different types of gratings in Fig. 1 the enhanced SERS signal is compared to the Raman signal of a single arbitrarily orientated molecule. The power density of the Stokes radiation for such a molecule, e.g., a molecule in a liquid with a refractive index  $n = 1$ , is

$$S_{\text{liquid}} = \frac{\pi^2 c}{2 \epsilon_0 \lambda^4 D^2} \overline{\alpha_R^2} |\vec{E}_0|^2. \quad (13)$$

$\overline{\alpha_R^2}$  is a space-averaged Raman polarizability, which is, e.g.,

$$\overline{\alpha_R^2} = [\frac{1}{2} (\alpha_{xx} + \alpha_{yy})]^2 \quad (14)$$

for diagonal Raman tensors.<sup>24</sup> Consequently, the molecular enhancement factor  $G_{\text{EM,mol}}$  is defined by

$$G_{\text{EM,mol}} = \frac{S_{\text{SERS,mol}}}{S_{\text{liquid}}} = \frac{|\vec{E}_s' \cdot \hat{\alpha}_R \cdot \vec{E}_0|^2}{|E_0|^4 \cdot \overline{\alpha_R^2}}. \quad (15)$$

In this investigation a diagonal Raman tensor with  $\alpha_{xx} = \alpha_{yy}$  is used. Because of this the influence of the  $90^\circ$  rotated orientation of the adsorbed molecules at the grating sides can be neglected. Furthermore, absolute values of the Raman tensor elements are thus not required because  $G_{\text{EM,mol}}$  is normalized with Eq. (14).

Section III shows that the SERS enhancement of single molecules depends on their location on the grating. In order to compare SERS signals for different gratings the averaged molecular enhancement factor,

$$G_{\text{EM}} = \frac{1}{N_{\text{mol}}} \sum_{m=1}^{N_{\text{mol}}} \frac{|\vec{E}_{s,m}' \cdot \hat{\alpha}_R \cdot \vec{E}_{0,m}|^2}{|E_0|^4 \cdot \overline{\alpha_R^2}}, \quad (16)$$

is defined. The sum in Eq. (16) considers all adsorption sites within one grating period and is divided by the number of adsorbed molecules  $N_{\text{mol}}$ . The sum is calculated with the emitted powers because of the incoherent nature of the spontaneous Raman emission. Therefore, the calculations can be confined to one grating period because the fields vary only with the phase factor  $\exp(jk_{xm}\Lambda)$  from period to period due to the Bloch periodicity.

$G_{\text{EM}}$  yields the SERS enhancement for emission into a single angle  $\theta_s$ . In practical experimental configurations, however, the emitted SERS signal is collected by a lens. For this reason an additional enhancement factor  $G_{\text{EM},\text{focus}}$  is defined, which describes measurements in the focal plane of a lens in backscattering geometry. The Gaussian beam of the incident laser light is focused by the lens on the grating at an angle  $\theta_0$ . The spot size of the focused laser beam is supposed to be large in comparison to the wavelength. Therefore, the light close to the focal plane is incident as a plane wave. The emitted SERS signal is collected by the lens within its acceptance angle  $2\Delta\theta$ . Thus, the detected signal in backscattering geometry is calculated by integrating Eq. (12),

$$S_{\text{EM},\text{focus}} = \int_{\theta_0 - \Delta\theta}^{\theta_0 + \Delta\theta} d\theta S_{\text{SERS},\text{mol}}, \quad (17)$$

and the corresponding average enhancement factor is

$$G_{\text{EM}} = \frac{\int_{\theta_0 - \Delta\theta}^{\theta_0 + \Delta\theta} d\theta \sum_{m=1}^{N_{\text{mol}}} |\vec{E}_{s,m}' \cdot \hat{\alpha}_R \cdot \vec{E}_{0,m}|^2}{N_{\text{mol}} |E_0|^4 \cdot \alpha_R^2 \cdot 2\Delta\theta}. \quad (18)$$

It should be noted that all definitions of enhancement factors in this section ( $G_{\text{EM},\text{mol}}$ ,  $G_{\text{EM}}$ , and  $G_{\text{EM},\text{focus}}$ ) give the electromagnetic enhancement per molecule. Differences between the definitions are only the averaging and the consideration of experimental configurations. Therefore, an enhancement effect due to an increasing number of molecules is not taken into account by these definitions. This additional effect can easily be considered by calculating the increasing surface within the laser spot for increasing grating depth or decreasing grating period.

### C. Surface plasmons

SERS is closely connected to the excitation of surface plasmons. For the first assessment of optimum angles of incidence we consider the plasmon dispersion relation on smooth surfaces,<sup>1</sup>

$$k_{\text{SP}} = \frac{\omega}{c} \sqrt{\frac{n_1^2 n_{\text{II}}^2}{n_1^2 + n_{\text{II}}^2}}, \quad (19)$$

with  $n_1 = n_{\text{air}}$  and  $n_{\text{II}} = n_{\text{Ag}}$ . For optical excitation of a surface plasmon  $k_{\text{SP}}$  has to meet the corresponding component  $k_x$  of the wave vector at the surface. The incident wave cannot meet this condition but one of diffracted orders may satisfy it. For example, on gratings with grating periods and wavelengths as considered in Sec. III resonant coupling of the first reflected order can be obtained. For this order the resonance condition is given by

$$k_{\text{SP}} = k_{x1} \quad (20)$$

where  $k_{x1}$  is defined by Eq. (4). Equation (20) allows estimation of the resonance angle

$$\theta_R = \arcsin \left[ \text{Re} \left( - \sqrt{\frac{n_1^2 n_{\text{II}}^2}{n_1^2 + n_{\text{II}}^2}} \right) + \frac{\lambda}{n_1 \Lambda} \right] \quad (21)$$

for surface plasmon excitation.<sup>10</sup> The calculated value is a good approximation only for flat gratings. Resonance angles for deep gratings can be obtained from the angular dependence of the Rayleigh coefficient  $R_1$  of the first reflected order. Furthermore, the dependence of  $R_1$  on the grating depth can be used to determine an optimum depth for plasmon resonance.<sup>18</sup>

## III. RESULTS

In Sec. III A both the excitation of the surface plasmon and surface-enhanced Raman scattering are considered for binary silver gratings with  $n_1 = n_{g1} = n_{\text{air}}$  and  $n_{\text{II}} = n_{g2} = n_{\text{Ag}}$ . Surface plasmon excitation is discussed in Sec. III A 1 for incident wavelengths of 700 nm and 800 nm. Corresponding refractive indices for silver of  $0.041 - i4.806$  and  $0.037 - i5.57$  have been calculated by interpolating experimental data<sup>27</sup> for these wavelengths. SERS on binary silver gratings is analyzed in Sec. III A 2 with 700 nm incident wavelength and 800 nm Stokes wavelength. This corresponds to a Raman shift of  $1781.25 \text{ cm}^{-1}$ . Grating depths are varied between 2 nm and 140 nm. The angle of incidence is varied in the range of  $0^\circ$  to  $20^\circ$ . Most of the calculations are obtained at a fixed grating period of 600 nm because resonance angles for incident and Stokes wavelengths are within the considered angular range for this period. SERS on silver gratings on flat silica substrates and on  $\text{SiO}_2$  gratings with silver layers is discussed in Sec. III B and Sec. III C with the same grating parameters for a direct comparison of the different grating types.

The convergence of RCWA critically depends on the order of the Rayleigh expansion. Convergent solutions for the Rayleigh coefficients are computed for 151 orders,<sup>22</sup> which correspond to Rayleigh coefficients from  $-75$  to  $75$ . The computation of the electric fields in the grating region is more critical. In order to achieve highly convergent solutions, 301 orders are used for calculation of the electric fields for binary silver gratings and silver gratings on flat silica substrates. For  $\text{SiO}_2$  gratings, however, a reduced number of 151 orders is used due to the higher computational times which are caused by the three-layer grating structure.

The relative convergence has been proven for all structures. Nevertheless, relative convergence does not necessarily indicate a correct solution of the scattering problem.<sup>28</sup> Therefore, near-field distributions have additionally been calculated by standard finite-difference time-domain methods.<sup>29</sup> They are in good agreement with results that have been computed by RCWA. Moreover, the reflected zeroth-order intensity has been measured for several grating configurations. The angular dependence of the experimental signals is in excellent agreement with the numerical results.<sup>30</sup> In this way the correctness of our RCWA results has been ensured.

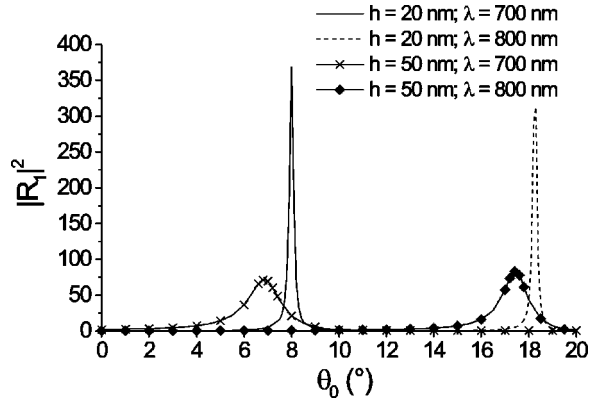


FIG. 4. Rayleigh coefficient  $|R_1|^2$  for 700 nm and 800 nm incident wavelengths  $\lambda$  on a binary silver grating with 600 nm grating period  $\Lambda$  and groove depths  $h$  of 20 nm and 50 nm as a function of the angle of incidence  $\theta_0$ .

### A. Binary silver gratings

#### 1. Surface plasmon excitation

In this investigation surface plasmon resonances are considered which are excited by the first reflected order (see Sec. II C). For a silver grating with 600 nm grating period Eq. (21) yields approximate resonance angles of  $8.29^\circ$  at  $\lambda_0 = 700$  nm and  $18.47^\circ$  at  $\lambda_s = 800$  nm. The exact angular dependence of the surface plasmons is obtained from the angular dependence of the corresponding Rayleigh coefficient  $|R_1|^2$  (Fig. 4).

The resonance angles are shifted to smaller values with increasing grating depth. Furthermore, the resonance height is reduced and the resonance is broadened with increasing groove depth. Figure 5 shows resonance angles and angular resonance widths in dependence on the grating depth. The resonance width  $2\Delta\theta_R$  is defined as the full width at half maximum.

Optimum plasmon excitation corresponds to a maximum resonance height of  $|R_1|^2$  and is obtained for small grating depths.<sup>18</sup> Values of  $|R_1|^2$  up to 700 have been calculated for grating depths between 11 nm and 12 nm. The maximum of  $R_1$  coincides with a minimum of the zero-order  $R_0$ , as expected from energy conservation. Therefore, surface plasmon

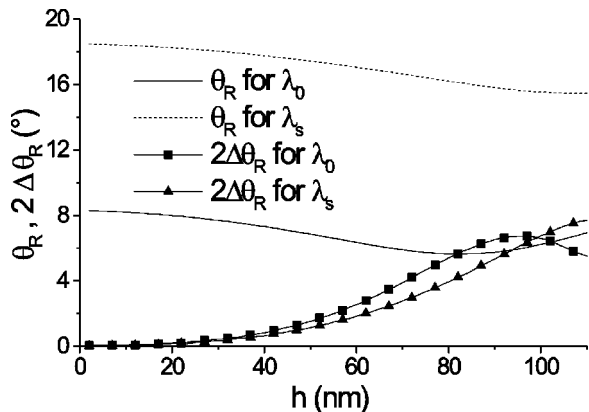


FIG. 5. Resonance angle  $\theta_R$  and resonance width  $2\Delta\theta_R$  for a silver grating with a period of  $\Lambda = 600$  nm as a function of the grating depth  $h$ .

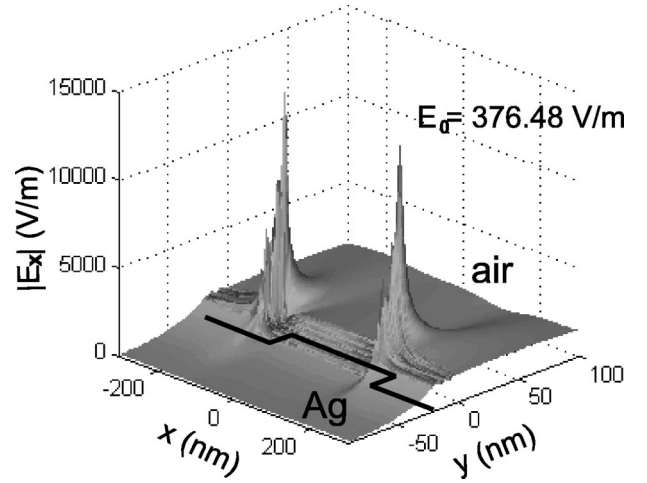


FIG. 6.  $E_x$  field at a silver grating with  $\Lambda = 600$  nm grating period,  $\lambda = 700$  nm wavelength, and  $h = 20$  nm grating depth for an angle of incidence  $\theta_0 = \theta_R = 8^\circ$ .

excitation results in a reflectance dip at resonance conditions<sup>19</sup> because the zero order is the only propagating order. The incident light completely couples into the surface plasmon which is propagating along the surface. Thereby, the resonance of  $R_1$  induces high evanescent electric fields at the absorption sites of the Raman-active molecules (see Fig. 6).

The dominance of the evanescent first order can be recognized in the electric near fields. The  $1/e$  decay lengths  $L_{1/e,\zeta}$  of the first order in region  $\zeta$  can be calculated from the imaginary part of the  $k_y$  component of the wave vector,

$$L_{1/e,\zeta} = \frac{1}{|\text{Im}(k_{\zeta,y})|}. \quad (22)$$

This yields  $1/e$  decay lengths of 505.08 nm in air (region I) and 22.67 nm in silver (region II). The rather high  $1/e$  length in air causes a weak dependence of SERS enhancement factors on the distance of the molecule from the surface. For calculations in Sec. III A 2 a distance of 0.5 nm is used, which is approximately the diameter of a benzene ring.

The tangential field close to the surface almost vanishes because silver is an excellent conductor. Therefore, only the perpendicular field components are enhanced. For this reason  $E_x$  is enhanced at the grating sidewalls (see Fig. 6). Conversely,  $E_y$  is enhanced at the top of the grating ridges and the bottom of the grooves. Calculation of  $E_y$  for the conditions of Fig. 6 yields values of  $|E_y| \approx 10^4$  V m<sup>-1</sup> at both the bottom and top sides. The different enhancement of  $E_x$  and  $E_y$  at horizontal and vertical grating surfaces would considerably influence SERS signals if Raman tensors with different components  $\alpha_{xx}$  and  $\alpha_{yy}$  were concerned. In this investigation the effect has only minor influence due to the choice of the Raman tensor.

$E_x$  is especially large at the upper grating edges (see Fig. 6). For  $E_y$  an additional local enhancement is also obtained at the top of the grating ridges close to the grating edges. This edge effect generally occurs for any angle of incidence and is not caused by surface plasmon excitation. Surface plasmons result in enhancement of the electric fields at all adsorption sites.

## 2. Surface-enhanced Raman scattering

The enhancement of electric near fields at the absorption sites of the molecules results in enhanced Raman signals from the surface. In order to consider the influence of plasmon excitation on SERS, enhancement factors as defined in Sec. II B are calculated for 700 nm incident wavelength and 800 nm Stokes wavelength. It is obvious from the electric fields in Fig. 6 that the contribution of single molecules to the overall SERS enhancement depends on their adsorption sites. For this reason the enhancement factor of single molecules  $G_{EM,mol}$  defined in Eq. (15) has been considered at different absorption sites along the surface at a distance of 0.5 nm for a 20 nm deep grating and optimum angle of incidence and emission angle. At the bottom of the grating grooves and the top of the ridges, enhancement factors of  $G_{EM,mol} \approx 2 \times 10^5$  have been calculated as long as the location is not close to the grating edges. Close to the grating edges the enhancement factor is one order of magnitude larger. Nevertheless, the average enhancement factor  $G_{EM}$  is about  $2 \times 10^5$  again, because there are far fewer molecules adsorbed at the grating edges than at the rest of the grating. Experimentally fabricated gratings will not have the exact rectangular shape considered here. Therefore, average enhancement factors are reasonable for comparison with experimental results because an overall enhancement is responsible for SERS.

For calculation of the averaged enhancement factor  $G_{EM}$ , a step size of 2 nm between the molecules parallel to the surface has been used. The experimental molecule density is most probably higher but a smaller step size increases the computational time and has only a small influence on average enhancement per molecule. A larger step size, however, influences the calculation of  $G_{EM}$  and has not been used for this reason.

In order to obtain maximum average enhancement factors  $G_{EM}$ , the angle of incidence  $\theta_0$  has to be the plasmon resonance angle of the incident wavelength  $\lambda_0$ . Due to additional coupling of the Raman scattered light to surface plasmons, the most enhanced SERS signals are emitted in the direction of the resonance angles  $\theta_s$  and  $-\theta_s$  for the Stokes wavelength  $\lambda_s$ . This angular dependence has already been considered in numerous theoretical and experimental investigations (see, for example, Refs. 10–12, 16, and 31). For this reason we discuss the influence of the grating depth  $h$  on the average enhancement factor  $G_{EM}$  only at a configuration with a single optimum angle of incidence and a single optimum emission angle. As surface plasmon resonance angles depend on the grating depth (see Fig. 5), the optimum angles have to be adjusted for each depth. Figure 7 exhibits  $G_{EM}$  for grating depths between  $h = 2$  nm and  $h = 110$  nm at resonance angles from Fig. 5. We have tested by additional calculations of  $G_{EM}$  that these angles actually result in the maximum enhancement factor for each depth.

Flat gratings yield higher SERS enhancements due to optimum plasmon excitation. For grating depths of about 11 nm average molecular enhancement factors of more than  $4 \times 10^5$  are achieved. However, this requires very accurate adjustments of both the angle of incidence and the detection angle. For the calculation of Fig. 7 resonance angles have been evaluated with an accuracy of  $0.01^\circ$ . Nevertheless, the

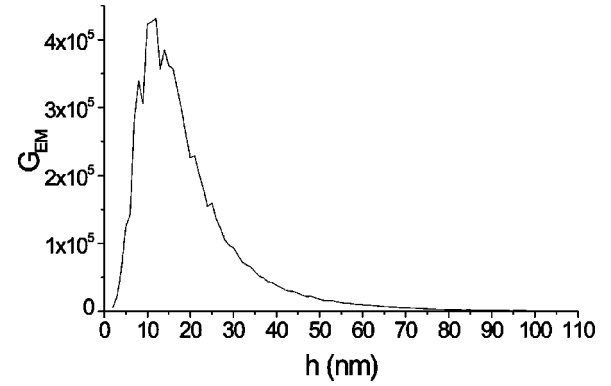


FIG. 7. Average molecular enhancement factor  $G_{EM}$  for 600 nm grating period as a function of grating depth  $h$ . Angle of incidence  $\theta_0$  and detection angle  $\theta_s$  are optimized for each depth (see Fig. 5).

convergence of  $G_{EM}$  is slow in the range of 5 nm to 20 nm grating depth.

The maximum SERS signal is detected at an emission angle that corresponds to the plasmon resonance angle at the Stokes wavelength. Furthermore, the angular width of the signal is given by the plasmon resonance width  $2\Delta\theta_R$  for  $\lambda_s$ , which increases for larger grating depths (see Fig. 5). Therefore, SERS signals from deep gratings are emitted into a larger angular range. This has to be taken into account if experimental enhancement factors are compared to calculated enhancement factors,<sup>12</sup> because a configuration with a single detection angle is not useful experimentally. For practical reasons the emitted signal is collected by a lens. Figure 8 shows the calculated factor  $G_{EM,focus}$  defined by Eq. (18), which corresponds to measurements in backscattering geometry. The angle of incidence  $\theta_0$  is varied in the range of  $0^\circ$  to  $20^\circ$ . The emitted signal is integrated from  $\theta_0 - 20^\circ$  to  $\theta_0 + 20^\circ$ . Thereby, SERS signals from deep gratings become comparable to SERS signals from a 20 nm deep grating and accurately adjusted angle of incidence (see Fig. 8).

The maximum enhancement factor in backscattering geometry  $G_{EM,focus}$  is about  $2 \times 10^3$  for a 20 nm deep grating. Thus,  $G_{EM,focus}$  is reduced by two orders of magnitude in comparison to the enhancement factor  $G_{EM}$  at a single detection angle (see Fig. 7). Nevertheless, this does not mean that a lower signal from the grating is detected. Obviously, the

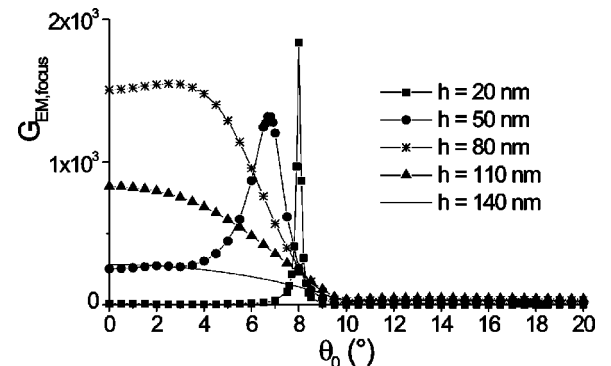


FIG. 8. Enhancement factor  $G_{EM,focus}$  for backscattering measurements on silver gratings with 600 nm grating period and various grating depths versus the angle of incidence  $\theta_0$ . The emitted signal is integrated over a detection angle from  $\theta_0 - 20^\circ$  to  $\theta_0 + 20^\circ$ .

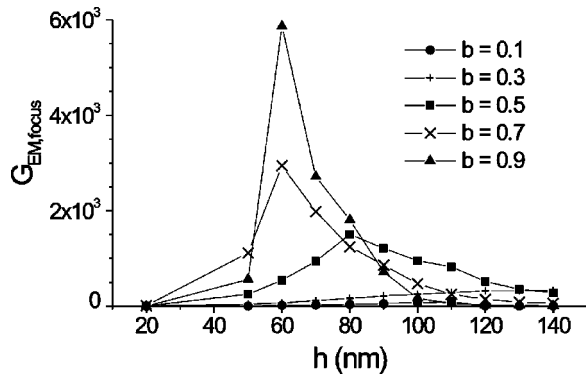


FIG. 9. Enhancement factor  $G_{EM,focus}$  at normal incidence as a function of  $b$ . The other grating parameters are as in Fig. 8.

signal intensity at the detector will be increased if the signal is collected by a lens. The increase of detected signal intensity, however, is larger for the isotropic signal from a liquid which is used as reference. For this reason the acceptance angle of the detection lens has to be taken into account precisely if SERS signals from gratings are compared to reference SERS signals, e.g., from a liquid or a flat silver surface.<sup>12</sup>

Due to the dependence on the detection system, general SERS enhancement factors cannot be given for grating-type substrates. Therefore, the influence of the grating geometry on the enhancement has to be considered also with respect to the experimental configuration. For this reason a general discussion of grating parameters is not useful. Here, we only show the influence of the ratio  $b$  of the grating ridge width to the grating period (see Fig. 1) on  $G_{EM,focus}$  at normal incidence (Fig. 9). A reduced groove width will considerably increase the SERS enhancement if the optimum grating depth is adjusted to the ratio  $b$ . Additional enhancement of SERS signals has already been experimentally investigated for asymmetric gratings with a reduced groove width.<sup>14</sup> The confirmation of this effect by numerical calculations is a new result to our knowledge.

### 3. Optimum grating structure for SERS measurements

In the last section we discussed several effects that have to be taken into account for comparison to an experimental investigation of SERS on binary silver gratings. An optimum grating depth for maximum enhancement has not been proposed because SERS depends not only on the grating structure but also on the experimental configuration. Therefore, the optimum grating structure can only be determined with regard to the application. Here, we consider practical aspects of SERS measurements in backscattering geometry. This involves large signal enhancement as well as stability and reproducibility of the measurements. In contrast to irregular roughened substrates, grating structures offer the possibility for reproducible SERS measurements due to the well-defined surface topology. However, this advantage will only be useful if the signal enhancement does not critically depend on the experimental configuration. For this reason deep gratings should be used in order to avoid the critical adjustment of the angle of incidence. Large SERS signals are obtained on both roughly adjusted deep gratings and accurately adjusted flat gratings (see Fig. 7).

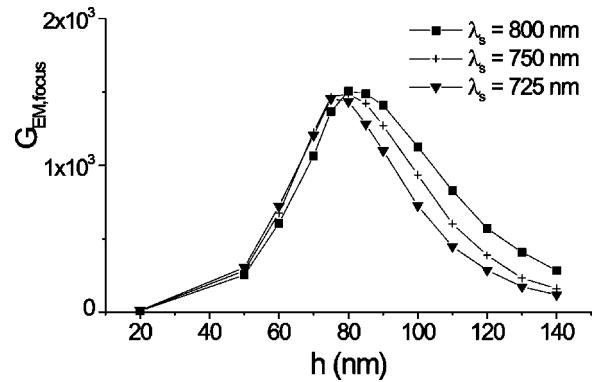


FIG. 10. Enhancement factor  $G_{EM,focus}$  for various Stokes wavelengths at normal incidence as a function of grating depth. The emitted signal is integrated over a detection angle from  $-20^\circ$  to  $20^\circ$ .

In the following, optimum grating structures are determined for SERS measurements in backscattering geometry without angle adjustment. Figure 10 shows  $G_{EM,focus}$  for normal incidence as a function of grating depth for different Stokes wavelengths of 800 nm, 750 nm, and 725 nm. These wavelengths correspond to Raman shifts of  $1781\text{ cm}^{-1}$ ,  $950\text{ cm}^{-1}$ , and  $491.4\text{ cm}^{-1}$  at an incidence wavelength of 700 nm. The optimum grating depth is about 85 nm. Experimentally, maximum SERS signals are observed at slightly deeper gratings of approximately 100 nm due to the increasing number of adsorbed molecules within the laser focus. Furthermore, the increasing number of molecules yields a slower decrease of SERS signals than of  $G_{EM,focus}$  in Fig. 10 for grating depths that are larger than 100 nm.

The optimum grating depth decreases for smaller Stokes wavelengths (see Fig. 10) because the resonance angles are shifted to lower values. Nevertheless, this dependence on the Raman shift is weak. Therefore, comparable SERS signals are obtained for all Raman bands in the considered experimental configuration without angular adjustment.

Furthermore, the grating period has only a small influence for such a configuration. On the contrary, for shallow gratings a different grating period will considerably influence the SERS signal because the angle of incidence is out of the resonance condition. For 100 nm grating depth, however, we calculated a decrease of the enhancement factor  $G_{EM,focus}$  by only a factor up to 5 for reduced grating periods down to 100 nm. Moreover, the dependence of the ratio  $b$  of grating ridge width to grating period is also weak for this grating depth (see Fig. 1). Consequently, we suggest that binary silver gratings with depths of about 100 nm should be used for stable and reproducible SERS measurements. The dependence on other grating parameters and the experimental configuration is weak for deep gratings. Additionally, SERS enhancement factors for measurements in backscattering geometry are comparable to that shallow gratings at adjusted angle of incidence.

### B. Silver gratings on flat silica substrates

In this section silver gratings on flat silica substrates are considered [see Fig. 1(b)]. This configuration is a 1D approximation for the properties of regular 2D arrays of nano-

TABLE I. Radiating reflected and transmitted orders for a silver grating on silica grating with a grating period of 600 nm.

$\lambda$	$\theta_0$	Radiating orders
700 nm	$0^\circ < \theta_0 < 9.59^\circ$	$R_0, T_0, T_1,$ and $T_{-1}$
	$9.59^\circ < \theta_0 < 16.76^\circ$	$R_0, T_0, T_1, T_{-1},$ and $R_1$
	$16.76^\circ < \theta_0 < 61.44^\circ$	$R_0, T_0, T_1,$ and $R_1$
	$\theta_0 > 61.44^\circ$	$R_0, T_0, T_1, R_1,$ and $T_2$
800 nm	$0^\circ < \theta_0 < 6.89^\circ$	$R_0, T_0, T_1,$ and $T_{-1}$
	$6.89^\circ < \theta_0 < 19.46^\circ$	$R_0, T_0,$ and $T_1$
	$19.46^\circ < \theta_0 < 90^\circ$	$R_0, T_0, T_1,$ and $R_1$

particles with a cross section equal to the line width of the grating. Such arrays of nanoparticles have been fabricated and tested experimentally.<sup>14</sup> In contrast to binary silver gratings the substrate refractive index  $n_{II}$  is real with  $n_{SiO_2} = 1.455$  at  $\lambda = 700$  nm and  $n_{SiO_2} = 1.453$  at  $\lambda = 800$  nm.<sup>32</sup> This causes differences in the propagation characteristics of the transmitted orders. For binary silver gratings only the zero reflected order is nonevanescence for angles of incidence up to  $9.59^\circ$ . On the contrary, for silver gratings on silica nonevanescence transmitted waves exist for all angles of incidence. Table I shows the propagating orders for wavelengths of 700 nm and 800 nm.

For a direct comparison with binary silver gratings the enhancement factor  $G_{EM}$  is calculated for a grating period of 600 nm. In the range from  $0^\circ$  to  $20^\circ$   $G_{EM}$  exhibits two resonances at angles  $9.59^\circ$  and  $19.46^\circ$  and two additional smaller ones at  $6.89^\circ$  and  $16.76^\circ$  (see Fig. 11). These resonances are not localized plasmon resonances but grating-induced resonances as discussed in Ref. 15. They occur when a reflected or transmitted order changes from radiating to evanescent or vice versa. Here, the small resonances are caused by a change of the propagation behavior of  $T_{-1}$  (see Table I).

The first strong resonance at  $9.59^\circ$  is due to a change of propagation behavior of  $R_1$  at the incidence wavelength and the second strong resonance corresponds to a change of  $R_1$  at the Stokes wavelength (see Table I). Consequently, maximum SERS signals are obtained for a  $9.59^\circ$  angle of inci-

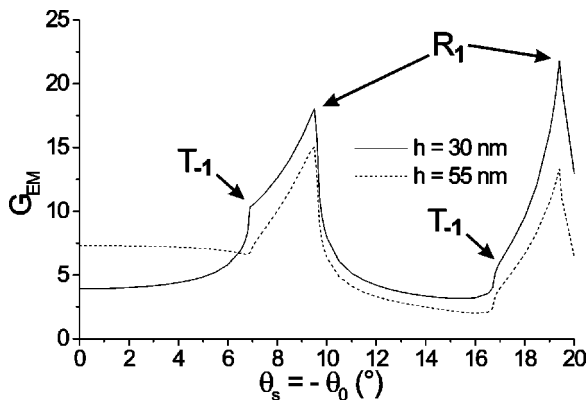


FIG. 11. Average molecular enhancement factor  $G_{EM}$  for a silver grating on silica with 600 nm grating period and grating depths of 30 nm and 55 nm as a function of the angle of incidence  $\theta_0$ . The emitted signal is detected at  $\theta_s = -\theta_0$ . The origins of the resonance ( $R_1$  and  $T_{-1}$ ) are indicated in the figure.

dence and detection angles of  $19.46^\circ$  and  $-19.46^\circ$ . For both grating depths in Fig. 11 a maximum value  $G_{EM}$  of about 60 has been calculated at these conditions. These small SERS enhancements at a single angle of incidence and a single detection angle in comparison to binary silver gratings lead to smaller enhancement factors  $G_{EM, \text{focus}}$  for the backscattering configuration. An enhancement factor  $G_{EM, \text{focus}}$  of about 10 has been calculated for both gratings of Fig. 11 at normal incidence. One reason for this small enhancement may be the large grating period of 600 nm, because optimum plasmon resonances are proposed for smaller isolated particles.<sup>33</sup> Structural dimensions, however, have only a small influence for an incident wavelength of 700 nm. For this wavelength variations of the grating period result in an optimum grating period of 200 nm with a corresponding  $G_{EM, \text{focus}}$  of 30.

Optimum localized plasmon excitation on single isolated particles will be obtained only if both the structural dimensions and the incident wavelength are reduced.<sup>33</sup> Therefore, we consider the dependence of  $G_{EM}$  on the wavelength for a grating with a grating period of 10 nm and a grating depth of 5 nm.  $G_{EM}$  exhibits a resonance for an incident wavelength of 410 nm for such a particle. For this incident wavelength enhancement factors  $G_{EM, \text{focus}}$  are about  $4 \times 10^2$ ,  $3 \times 10^2$ , and  $2 \times 10^2$  for Stokes wavelengths of 420 nm, 430 nm, and 440 nm, which correspond to Raman shifts of  $579 \text{ cm}^{-1}$ ,  $1131 \text{ cm}^{-1}$ , and  $1658 \text{ cm}^{-1}$ . It should be noted that these enhancement factors are valid for 1D gratings. For small particles with a cross section of 5 nm in the direction of the  $z$  axis this is a rough approximation. Therefore, the quantitative validity of enhancement factors of about  $3 \times 10^2$  for very small particles has to be carefully considered. Nevertheless, an increasing SERS enhancement for smaller wavelengths and particle dimensions and a stronger dependence on the Raman shift are qualitatively proposed by our model.

### C. Silver on $SiO_2$ gratings

Strong enhancement factors for silver gratings on dielectric substrates can only be achieved for suitable incident wavelengths and with grating dimensions that are optimized for localized plasmon resonances. For an incident wavelength of 700 nm, however, even the electromagnetic coupling between the grating lines does not considerably improve the performance. One reason for this is that the resonance condition in Sec. III B has been obtained only from the propagation characteristic of the resonant order. A phase matching condition for this order has not been considered. Therefore, the basic idea for the structure of Fig. 1(c) with two vertically offset gratings is the possibility of using an additional phase shift in order to induce a different collective plasmon resonance. Thus, interaction between these two layers can cause much stronger electromagnetic fields and thereby higher SERS enhancements. Figure 12 shows the enhancement factor  $G_{EM, \text{focus}}$  for backscattering measurements on a 70 nm deep grating with various heights of the silver lines. Considering suitable fabrication methods the silver line heights of top and bottom layers are identical.

For normal incidence, SERS enhancement is comparable to that in deep binary silver gratings and thereby two orders of magnitude larger than the enhancement for a single silver grating layer. There are two different grating conditions that

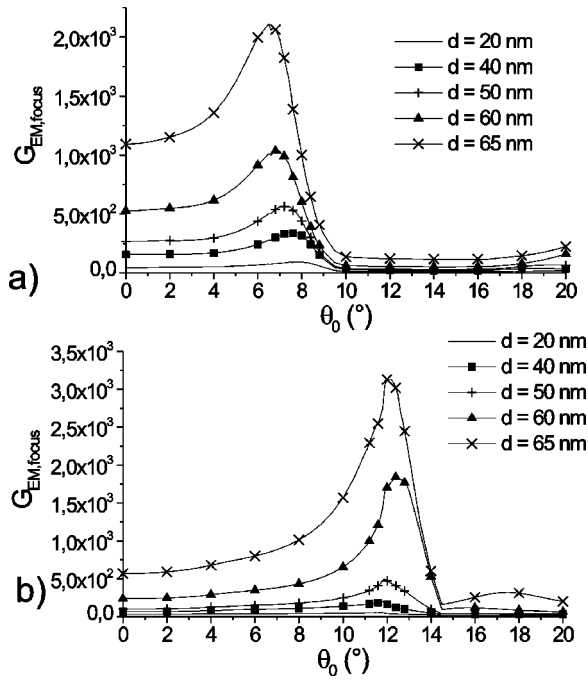


FIG. 12. Enhancement factor  $G_{EM,focus}$  for backscattering measurements on  $\text{SiO}_2$  gratings with a grating depth of 70 nm and different silver layer thicknesses  $d$  as a function of the angle of incidence  $\theta_0$  (a) with a grating period of  $\Lambda = 600$  nm and (b) with a grating period of  $\Lambda = 560$  nm.

cause maximum enhancements. For silver line heights slightly smaller than the grating depth, the increased interaction due to the narrow distance between bottom and top particles results in enhanced signals (see Fig. 12). This effect has also been tested for other grating depths. Furthermore, especially large SERS signals are obtained for an angle of incidence that is close to the resonance angle of the first reflected order. For these resonances integrated enhancement factors of about  $2 \times 10^3$  have been calculated for various grating periods and grating depths with slightly smaller silver layer thicknesses.

The resonance angle depends on the ratio of silver layer thickness to grating depth. Both optimum angle of incidence  $\theta_0$  and emission angle  $\theta_{s,max}$  are shifted from the resonance angles for a single-layer grating (see Fig. 11) by up to  $2^\circ$  with increasing silver layer thickness. Figure 13 shows the enhancement factor  $G_{EM}$  as a function of detection angle with the optimum angle of incidence  $\theta_0$  for each grating. An enhancement factor  $G_{EM}$  up to  $10^4$  is obtained in the direction of the optimum emission angle. This maximum enhancement factor is one order of magnitude lower than the maximum  $G_{EM}$  for a shallow binary silver grating (see Fig. 7). Nevertheless, the emission angular width is about  $3^\circ$  and thus much larger than for the binary silver grating. Moreover, the resonance of the transmitted negative first order yields considerable enhancement due to the additional coupling between the layers. Thus, a double resonance with comparable broad angular widths and additionally good enhancement for the nonresonant emission angles cause the large integrated enhancement factor for measurements in backscattering geometry on  $\text{SiO}_2$  gratings.

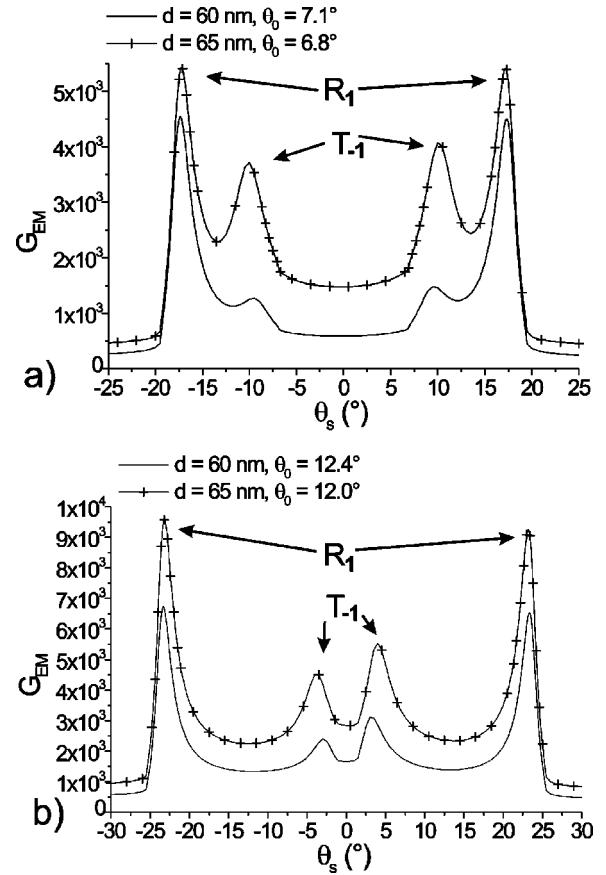


FIG. 13. Enhancement factor  $G_{EM}$  as a function of detection angle on  $\text{SiO}_2$  gratings with grating periods of (a) 600 nm and (b) 560 nm, a grating depth of 70 nm, silver layer thicknesses of 60 nm and 65 nm, and angles of incidence  $\theta_0$  that correspond to the resonance angles for the incident wavelength  $\lambda_0$ .

#### IV. DISCUSSION

Surface plasmon excitation on rectangular binary silver gratings has been considered in dependence on incident wavelength, grating period, ratio of grating ridge width to grating period, and grating depth. For shallow gratings resonance angles can be calculated from the approximate Eq. (21). With increasing grating depth resonance angles are shifted to smaller values and have to be obtained from the resonance of  $|R_1|^2$ . For deep gratings the angular adjustment is less critical due to increasing resonance widths.

Maximum surface plasmon excitation is obtained for shallow gratings with depths between 10 nm and 20 nm. This coincides well with investigations of sinusoidal gratings, which propose an optimum depth of 25 nm.<sup>18</sup> The slight difference may be caused by the different grating shape as well as by the different values of grating period and incident wavelength used in this investigation. The optimized grating depth for surface plasmon excitation yields high average molecular SERS enhancement up to  $4 \times 10^5$ . However, this requires a very exact adjustment of the angle of incidence and detection angle, which is obvious from the lower convergence in the range of 5 nm to 20 nm grating depth (see Fig. 7). The strong dependence on exact angular adjustment is also valid in experimental measurements on flat gratings.

SERS enhancement factors of single molecules vary depending on their adsorption sites within the grating. Electric

fields are particularly enhanced at grating edges, and molecules at these sites emit SERS signals that are additionally increased by one order of magnitude. Nevertheless, the average molecular enhancement on a silver grating is dominated by molecules on the top of the grating ridges and the bottom of the grating grooves due to their larger number. For this reason SERS on silver gratings is not an edge effect but a collective effect which is caused by collective surface plasmon excitations.

SERS on silver gratings is also a long range effect because the evanescent plasmon fields have  $1/e$  decay lengths of about 500 nm in air. In contrast, numerical models for SERS on isolated metal particles predict a strong dependence on the distance from the metal surface due to the excitation of localized surface plasmons.<sup>3</sup> The weaker dependence on the distance of the Raman-active molecules at silver gratings may be useful in certain applications, e.g., for SERS measurements with several molecule layers or on surfaces with additional chemical coatings for a selective adsorption of the molecules.<sup>34</sup>

Experimental configurations for Raman measurements generally have a detection system with lenses in order to collect the emitted intensity. This has to be considered when comparing measured and calculated enhancement factors.<sup>12</sup> Here, we consider the influence of the experimental configuration on the calculated enhancement factor. A larger acceptance angle has only a minor influence on the enhancement for shallow gratings due to the narrow resonance width. On the contrary, increasing resonance widths for increasing grating depths will result in higher observed signals if the emitted signal is collected by a lens. This is especially obvious for a grating depth of 80 nm, for which the integrated enhancement factor at normal incidence is only slightly smaller than that for a 20 nm deep grating and optimized angle of incidence (see Fig. 10). For this reason we propose that deep gratings should be used for experimental Raman measurements in backscattering geometry. The average molecular enhancement factor is comparable but the adjustment of the angle of incidence is less critical. Especially for measurements without angular adjustment, e.g., for normal incidence, deep gratings exhibit much larger SERS enhancements. This corresponds well with experimental investigations reporting maximum SERS signals for grating depths of more than 100 nm.<sup>14</sup> The fact that slightly larger grating depths are optimum in experimental measurements can be explained by the increasing number of absorbed molecules in the focus due to additional adsorption sites at the larger sidewalls.

On the other hand, reduced groove widths at fixed grating periods do not influence the number of molecules. For this reason the effect of a higher enhancement at these groove widths will generally be observed. Again, this is confirmed by experimental results.<sup>14</sup>

Silver gratings on silica substrates are a 1D approximation for the properties of regular arrays of nanoparticles with cross sections equal to the linewidth. For these silver gratings on silica SERS enhancement factors have been calculated that are two orders of magnitude smaller than those for binary silver gratings with comparable structural dimensions. Thereby, the low signal enhancement of SERS measurements on regular arrays of nanoparticles<sup>14</sup> can be explained.

It should be noted, however, that the enhancement of isolated particles strongly depends on the particle size and the incident wavelength. Here, structures with grating periods of more than 100 nm and an incident wavelength of 700 nm have been regarded because they have been used for experimental measurements. For these conditions the resonances involved are purely grating-induced resonances as described in Sec. III B. For smaller particles and shorter wavelengths, isolated particle plasmon resonances are excited<sup>33</sup> and thus higher SERS signals are proposed.

Electromagnetic interaction between closely spaced particles can result in increased SERS signals.<sup>35</sup> Here, double silver layers on SiO<sub>2</sub> gratings exhibit very high SERS signals due to the resonant coupling between the layers. This is obvious from the influence of both the layer thickness and the grating depth on optimum angle of incidence and emission angle, which differ from the angles for a single layer. The enhancement of SERS signals is increased by two orders of magnitude in comparison to a grating with a single silver layer at normal incidence and is comparable to the enhancement for optimum binary silver gratings. This increased enhancement at normal incidence has also been observed experimentally.<sup>14</sup> Moreover, very large enhancement factors will be obtained if the silver layer thickness is only slightly smaller than the grating depth and the angle of incidence is close to the resonance angle of the first diffracted order. This condition results in increased enhancement in comparison to optimum binary silver gratings and yields additionally larger resonance widths for the angle of incidence. Due to these superior properties SiO<sub>2</sub> gratings are the most interesting grating-type substrate for SERS.

## V. CONCLUSION

A general method for the calculation of surface plasmon excitation and surface-enhanced Raman scattering on rectangular grating structures has been presented. The numerical analysis of different grating types as well as of gratings with different structural parameters yields SERS enhancement factors between 10 and 10<sup>5</sup> depending both on the grating structure and on the experimental configuration. The dependence of calculated enhancement factors on grating period, grating depth, silver layer thickness, angle of incidence, and emission angle is in accordance with experimental results.<sup>14</sup> In particular, the experimentally observed increasing enhancement at binary silver gratings with depths of more than 80 nm is explained by considering a realistic experimental configuration involving a lens for detection. Thereby, the increasing resonance widths of the surface plasmons at deep gratings play an important role at nonadjusted angles of incidence and detection. We suggest from our theoretical consideration that deep silver gratings with grating depths of about 100 nm should generally be used for reproducible SERS measurements in backscattering geometry. The SERS enhancement is comparable to that at shallow gratings but the dependence on other grating parameters and the experimental configuration is rather weak.

SERS enhancement factors up to  $5 \times 10^5$  are calculated on binary silver gratings for Stokes emission into a single direction. Due to the different angular widths, however, SERS

enhancement factors have to be calculated in dependence on experimental configurations for the comparison of different grating types. Here, we considered measurements in back-scattering geometry and a detection lens with an acceptance angle of  $2\Delta\theta=40^\circ$ . Grating periods have been varied between 100 nm and 600 nm and the incident wavelength has been fixed at 700 nm. For this experimental configuration and structural dimensions enhancement factors for silver

gratings on flat silica substrates are two orders of magnitude smaller than for binary silver gratings, where factors of about  $10^3$  are calculated. On the contrary, double silver gratings on silica exhibit increased enhancement in comparison to binary silver gratings due to coupling effects between the layers. Due to additional larger resonance widths these structures are very interesting for further theoretical and experimental investigations of SERS.

- 
- <sup>1</sup>H. Raether, *Surface Plasmons* (Springer-Verlag, Berlin, 1988).  
<sup>2</sup>M. Moskovits, *Rev. Mod. Phys.* **57**, 783 (1985).  
<sup>3</sup>A. Wokaun, *Solid State Phys.* **38**, 223 (1984).  
<sup>4</sup>S. Angel, T. Kulp, M. Myrick, and K. Langry, *Chem. Sens. Technol.* **3**, 163 (1991).  
<sup>5</sup>J. Bello, V. Narayanan, D. Stokes, and T. Vo-Dinh, *Anal. Chem.* **62**, 2437 (1990).  
<sup>6</sup>C. Viets and W. Hill, *Sens. Actuators B* **51**, 92 (1998).  
<sup>7</sup>*Surface Enhanced Raman Scattering*, edited by R. Chang and T. Furtak (Plenum Press, New York, 1982).  
<sup>8</sup>P. Liao *et al.*, *Chem. Phys. Lett.* **82**, 355 (1981).  
<sup>9</sup>P. Liao, in *Surface Enhanced Raman Scattering* (Ref. 7), pp. 379–390.  
<sup>10</sup>A. Girlando *et al.*, *J. Chem. Phys.* **72**, 5187 (1980).  
<sup>11</sup>J. Tsang, J. Kirtley, and T. Theis, *Solid State Commun.* **35**, 667 (1980).  
<sup>12</sup>I. Baltog, N. Primeau, and R. Reinisch, *Appl. Phys. Lett.* **66**, 1187 (1995).  
<sup>13</sup>M. Kahl, E. Voges, and W. Hill, *Spectrosc. Europe* **10**, 8 (1998).  
<sup>14</sup>M. Kahl *et al.*, *Sens. Actuators B* **51**, 285 (1998).  
<sup>15</sup>H. Lehmann *et al.*, *J. Vac. Sci. Technol. B* **1**, 1207 (1983).  
<sup>16</sup>M. Arnold *et al.*, *J. Mod. Opt.* **39**, 2329 (1992).  
<sup>17</sup>K. Carron *et al.*, *J. Opt. Soc. Am. B* **3**, 430 (1986).  
<sup>18</sup>M. Nevriere and R. Reinisch, *Phys. Rev. B* **26**, 5403 (1982).  
<sup>19</sup>R. Petit, *Electromagnetic Theory of Gratings* (Springer-Verlag, Berlin, 1980).  
<sup>20</sup>M. Moharam, E. Grann, D. Pommet, and T. K. Gaylord, *J. Opt. Soc. Am. A* **12**, 1068 (1995).  
<sup>21</sup>L. Li and C. Haggans, *J. Opt. Soc. Am. A* **10**, 1184 (1993).  
<sup>22</sup>P. Lalanne and G. Morris, *J. Opt. Soc. Am. A* **13**, 779 (1996).  
<sup>23</sup>L. Li, *J. Opt. Soc. Am. A* **13**, 1870 (1996).  
<sup>24</sup>D. Long, *Raman Spectroscopy* (McGraw-Hill, New York, 1977), pp. 48–61.  
<sup>25</sup>J. Kong, *Theory of Electromagnetic Waves* (John Wiley & Sons, New York, 1975), pp. 269–271.  
<sup>26</sup>J. Kong, *Electromagnetic Wave Theory* (John Wiley & Sons, New York, 1986), pp. 229–233.  
<sup>27</sup>D. Lynch and W. Hunter, in *Handbook of Optical Constants of Solids*, edited by E. Palik (Academic Press, San Diego, 1998), pp. 350–357.  
<sup>28</sup>Y. C. Shih, in *Numerical Techniques for Microwave and Millimeter-Wave Passive Structures*, edited by T. Itoh (John Wiley & Sons, New York, 1989), pp. 603–604.  
<sup>29</sup>A. Taflov, *Computational Electrodynamics: The Finite-Difference Time-Domain Method* (Artech House, Inc., Boston, 1995).  
<sup>30</sup>M. Kahl *et al.* (unpublished).  
<sup>31</sup>W. Knoll, M. Philpott, and J. Swalen, *J. Chem. Phys.* **75**, 4795 (1981).  
<sup>32</sup>H. Philipp, in *Handbook of Optical Constants of Solids* (Ref. 27), p. 760.  
<sup>33</sup>M. Kerker, D.-S. Wang, and H. Chew, *Appl. Opt.* **19**, 4159 (1980).  
<sup>34</sup>W. Hill *et al.*, *Anal. Chem.* **34**, 3187 (1995).  
<sup>35</sup>F. García-Vidal and J. Pendry, *Phys. Rev. Lett.* **77**, 1163 (1996).